IEEE Access
Multidisciplinary | Rapid Review | Open Access Journal

Received December 13, 2018, accepted January 16, 2019, date of publication January 30, 2019, date of current version February 27, 2019.

Digital Object Identifier 10.1109/ACCESS.2019.2896136

An Innovative Constant Voltage Control Method of PMSM-Type ISG Under Wide Engine Speed Range for Scooter With Idling Stop

MING-SHI HUANG[1], (Member, IEEE), KUAN-CHENG CHEN[1], TSE-KAI CHEN[1], YU-CHIANG LIANG[2], AND GUAN-YOU PAN[2]

[1]Department of Electrical Engineering, National Taipei University of Technology, Taipei 10608, Taiwan
[2]Sanyang Motor Co., Ltd., Hsinchu 30444, Taiwan

Corresponding author: Ming-Shi Huang (mingshi@gmail.com)

ABSTRACT The integrated starter generator (ISG) is used for an idling-stop scooter, which can effectively reduce both air pollution and fuel consumption during idle periods. The ISG, that is made using permanent magnet synchronous motor (PMSM), should provide enough torque for engine cranking, which causes the output voltage of a three-phase rectifier from the ISG to be higher than the battery voltage (12V) in generating mode. Hence, the output voltage control of the ISG cannot be performed by a conventional boost operation. This paper proposes a constant voltage control method for the PMSM type ISG in generating mode to generate a 12V dc-link voltage over a wide speed range of the engine. First, a phasor diagram is used to explain the principle of how the controlling of phase voltage lagging behind its back-EMF can achieve power generation. Furthermore, the relationships among generating dc-link voltage, generating power, phase voltage lagging angle, and current angle are derived for developing the control methodology. Due to the small lagging phase angles of the ISG in generating mode from light to rated load, a dc-link voltage controller with a feedforward angle control for the light load is adopted to yield voltage control with or without connected 12V battery. In addition, a dc-link current feedforward module is proposed to enhance the voltage controller without the 12V battery. Consequently, the voltage variation under step load change is further reduced to nearly 0V on the test bench and on a 150cc scooter. Finally, a DSP-based ISG drive is implemented to verify the effectiveness of the proposed method on both the test bench and the 150cc scooter.

INDEX TERMS Integrated starter generator (ISG), idling stop, six-step voltage operation, phasor analysis, PMSM, scooter.

I. INTRODUCTION

Due to growing demand for fuel efficiency and CO2 reduction, an idling-stop or start-stop system can be utilized to automatically shut down and crank an internal combustion engine (ICE) when the driver stops and starts, respectively, to reduce the ICE idling time while waiting at traffic lights. The technology can help by reducing vehicle fuel consumption up to 10% in urban test mode [1], [2] and up to 7% for scooters using the ECE R40 mode [3]. Moreover, the evaluated results in [4] show that idling-stop devices of motorcycles can reduce carbon monoxide emissions up to 36.9%. Additionally, an idling-stop system may use the existing 12V lead-acid battery or a low capacity Li-ion battery can be installed in other hybrid electric vehicles to fulfil required functions. Idling-stop system can lead to low cost of usage and is becoming popular in recently produced vehicles and scooters. Moreover, the Taiwan government encourages current ICE scooter makers to install an idling-stop module on scooter in 2017, and stipulates that at least 50% of ICE scooter models must have idling-stop function in 2022.

There are two types of idling-stop systems, which are categorized according to hardware structure. One type is the conventional system having separate starter and generator, and the other is an integrated starter generator within a single machine. The ISG approach provides several advantages [5], such as elimination of the starter, and the belt or pulley coupling between generator and engine, which reduces both cost and transmission loss. Hence, volume, noise, and vibration of an ISG are lower than in the conventional idling-stop system for providing quick- and quiet-restart ICE. However, an ISG can act as a starter or generator to meet the

The associate editor coordinating the review of this manuscript and approving it for publication was Bora Onat.

requirements of cranking the engine and producing electric power, which requires high torque and wide engine speeds, respectively [1], [6]. The required characteristics of an ISG may cause conflicts in electric machine design under limited battery voltage. The research in [1] examines main pros and cons of induction machine (IM), permanent magnet (PM) machine and reluctance machine for ISGs. Although the claw-pole belt driven ISG [6], [7], which is equipped with rotor winding for field-weakening control, can provide both high start torque and high speed operation [6], lower efficiency is the main drawback. Due to robust structure and low cost, IMs are applied to ISGs [8], [9]. However, IMs for ISGs need a larger air gap to meet vibrational constraint, which leads to reduce motor efficiency by larger magnetizing current and enlarged power capacity of the inverter [1].

On the other hand, PM machines are becoming popular for ISGs due to their higher efficiency and higher power density [10]–[22]. With dq-axis voltage commands as feedback for field-weakening on interior permanent magnet synchronous motor (IPMSM) in generating mode, the simulation results show that the proposed starter and alternator control module can provide good dc bus voltage (42V) during a worst-case step load condition at 6000rpm [10]. However, the control method is based on vector control and it is assumed that the flux saturation effect is not serious. The research in [18] uses synchronous rectification to replace the traditional boost-type generating control for ISG for enhanced efficiency. However, a dc-dc converter is still required to obtain a fixed dc-link voltage. Due to price issue, several studies and products [19]–[21] have applied low cost ferrite magnets to replace rare-earth magnets in PM motors. For increasing generated torque of ferrite PM ISGs, the outer rotor structure is adopted [19], [20]. Moreover, the core loss is reduced due to high electrical resistivity of the ferrite magnet in high current harmonics applications [19].

The researches in [18], [21], and [22] focus on ISGs for scooters with idling stop. The six-step voltage control method is used to generate good fixed dc-link voltage [21]. However, the study does not explain generating mechanism by the six-step voltage operation. For reducing size of ISG, the research in [22] uses a rare-earth PM for the outer rotor type motor. Therefore, the engine is to be cranked (i.e. started) faster due to low inertia of the rotor, but the generating mode is not addressed. The difference between the proposed technology and prior approaches are summarized in Table 1. Fig. 1 shows the function block and related waveforms of PMSM type ISG for the scooter under cranking and generating mode. The ISG is operated in generating mode when the engine runs from 1800 rpm to approximately 8000 rpm. As can be seen in Fig. 1(b), the output voltage of the three phase rectifier from the ISG is higher than dc-link voltage V_{dc}(12V). Hence, the dc-link voltage control cannot be performed by conventional vector control in generating mode for wide range engine speed. Moreover, many riders in the countryside of South Asia do not use batteries if the factory-equipped battery is damaged. Hence scooters sold in South Asia are usually equipped with a kick-start mechanism.

TABLE 1. Comparison of ISGs with proposed method (IM excluded).

Prior arts	ISG type	Generated fixed dc-link voltage method	Key characteristics
[6][7]	Claw pole	Control rotor winding current to yield variable excited flux	*Easy to reach fixed dc-link voltage under wide speed range *Low efficiency *Requires a current controller to yield required winding current
[10][13]	IPMSM rare earth	Vector control with d-q axis voltage feedbacks	*Uses single drive for both motoring and generating modes *[10] Does not consider the flux-saturation effect of IPMSM *[13] Considers the flux-saturation effect but only discusses motoring mode.
[18]	BLDC	Synchronous rectifier with a dc-dc converter	*Requires a dc-dc converter for generating mode
[21]	PMSM Outer rotor/ ferrite magnet	Six-step voltage operation without current regulators	*Uses single drive for both motoring and generating modes *Does not describe operating principal and control methodology
Proposed method	PMSM Outer rotor/ ferrite magnet	Six-step voltage operation without current regulators	*Uses single drive for both motoring and generating modes *Explains the principal of generating voltage *Derives the formula between generating power and voltage phase angle *Analyzes and designs voltage controller

This paper proposes a constant voltage control method for the PMSM type ISG to generate 12V dc-link voltage over a wide range of engine speeds for scooters with an idling stop system. The ISG is an outer-rotor PMSM with surface mounted ferrite PM and is equipped with three digital Hall sensors for detecting rotor position. Therefore, a six-step voltage operating method is proposed under generating mode to reach constant dc-link voltage. The phasor diagram of fundamental frequency is used to explain the principle for that voltage phase lagging behind the same phase back-EMF by θ_v can achieve power generation under different engine speeds The scooter load generally ranges from 25W to 130W for a 150cc scooter, which leads to smaller θ_v of the ISG in generating mode. Therefore, a dc-link voltage controller with a feedforward angle θ_b is adopted to yield good voltage control with or without connected a 12V battery. In addition, a dc-link current feedforward module is added to the voltage controller for scooter without a 12V battery, which allows the dc-link voltage to be maintained at 12V under a step load change. Finally, a DSP-based (TMS320F28035, Texas Instruments) ISG drive is implemented to verify the effectiveness of the derived methods on both the test bench and a 150cc scooter.

II. PRINCIPLE OF SIX STEP VOLTAGE OPERATION UNDER GENERATING MODE

The following assumptions are made to derive formulas for PMSM type ISG in generating mode under six-step voltage operation.

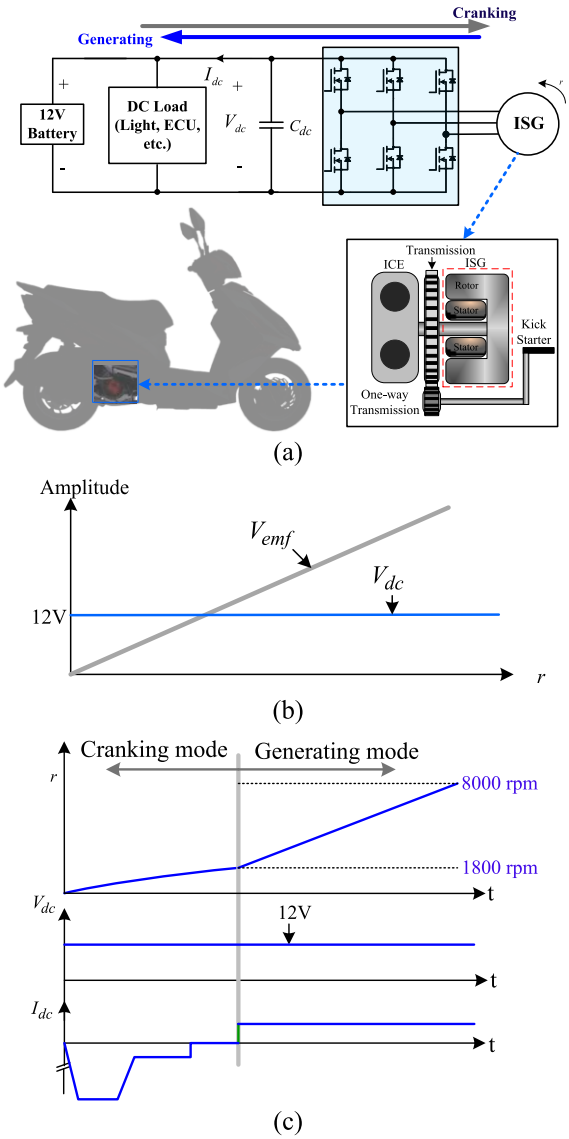

FIGURE 1. Typical function block and the related waveforms of PMSM type ISG for scooter; (a) function block, (b) amplitude of back-EMF and dc-link voltage vs. engine speed, (c) waveforms of ISG.

(i) No load back-EMF is sinusoidal;
(ii) The three phase electrical machine is balanced;
(iii) Flux saturation and parameters changes are neglected.

Let u phase back-EMF v_{emf_u} of the ISG be a reference. Then the u-phase six-step voltage v_{un} generated by motor drive can be illustrated as shown in Fig. 2(a). Wherein, θ_v is controlled by motor drive to provide the needed dc-link voltage for different loaded conditions and speeds in generating mode.

Hence u-phase voltage v_{un} can be expressed by a Fourier series as:

$$v_{un}(t) = v_{un1}(t) + \sum_{k=1,2,\ldots}^{\infty} V_{unk}[(6k \pm 1)\omega_e t + \theta_{vk}] \quad (1)$$

where

$$v_{un1}(t) = \frac{2}{\pi} V_{dc} \sin(\omega_e t + \theta_v)$$
$$V_{unk} = \frac{2}{(6k \pm 1)\pi} V_{dc}$$

v_{un1} is the fundamental voltage; V_{unk} is amplitude of kth order harmonics voltage; ω_e is electric angular speed which is equal to the ISG speed ω_r multiplied by the rotor magnet pole pairs; t is time in second; θ_{vk} is kth order phase voltage angle; V_{dc} is dc-link voltage, and θ_v is lagging angle of u-phase voltage generated by the drive.

It is obvious that the generating electric power is converted from the kinetic power of engine by the ISG based on fundamental frequency. Hence, the u-phase voltage equivalent circuit and phasor diagram can be derived and shown in Figs. 2(b) and (c), respectively. The fundamental phase current i_{un1}, u-phase generated power P_u and three phase generated average power P are derived as:

$$i_{un1}(t) = I_{un1} \sin(\omega_e t + \theta_{i1}) \quad (2)$$
$$P_u = \text{Real}(v_{un1} i_{un1})$$
$$= \frac{1}{\pi} V_{dc} I_{un1} [\cos(\theta_v - \theta_{i1}) - \cos(2\omega_e t + \theta_v + \theta_{i1})] \quad (3)$$
$$P = \frac{3}{\pi} V_{dc} I_{un1} \cos(\theta_v - \theta_{i1}) \quad (4)$$

where

$$I_{un1} = \sqrt{\frac{(\frac{2}{\pi} V_{dc} \cos\theta_v - V_{emf})^2 + (\frac{2}{\pi} V_{dc} \sin\theta_v)^2}{r_s^2 + (\omega_e L_s)^2}}$$
$$\theta_{i1} = 180^\circ + \tan^{-1} \frac{\frac{2}{\pi} V_{dc} \sin\theta_v}{\frac{2}{\pi} V_{dc} \cos\theta_v - V_{emf}} - \tan^{-1} \frac{\omega_e L_s}{r_s}$$
$$v_{emf_u}(t) = V_{emf} \sin(\omega_e t)$$
$$V_{emf} = k_e \omega_e \phi_m$$

I_{un1} is amplitude of the fundamental phase current; θ_{i1} is the fundamental current angle; V_{emf} is amplitude of the back-EMF; r_s is phase winding resistance; L_s is average inductance of phase winding, k_e is phase back-EMF constant; and ϕ_m is flux linkage generated by the ferrite magnet.

If θ_v is increased at the same speed, shown in Fig. 2(d), the three phase generated average power P is enlarged due to an increase of the angle between current and phase voltage. However, the generated power at the same θ_v under different speeds, as shown in Fig. 2(e), is not easily observed from the phasor diagram.

Since v_{emf_u} is higher than V_{dc} in high speed region, I_{un1} and θ_{i1} can be approximately expressed as a constant if r_s is considered to be negligible compared to $\omega_e L_s$, i.e.,

$$I_{un1} \approx \frac{V_{emf}}{\omega_e L_s} = k_e \frac{\phi_m}{L_s} \quad (5)$$
$$\theta_{i1} \approx 90^\circ \quad (6)$$

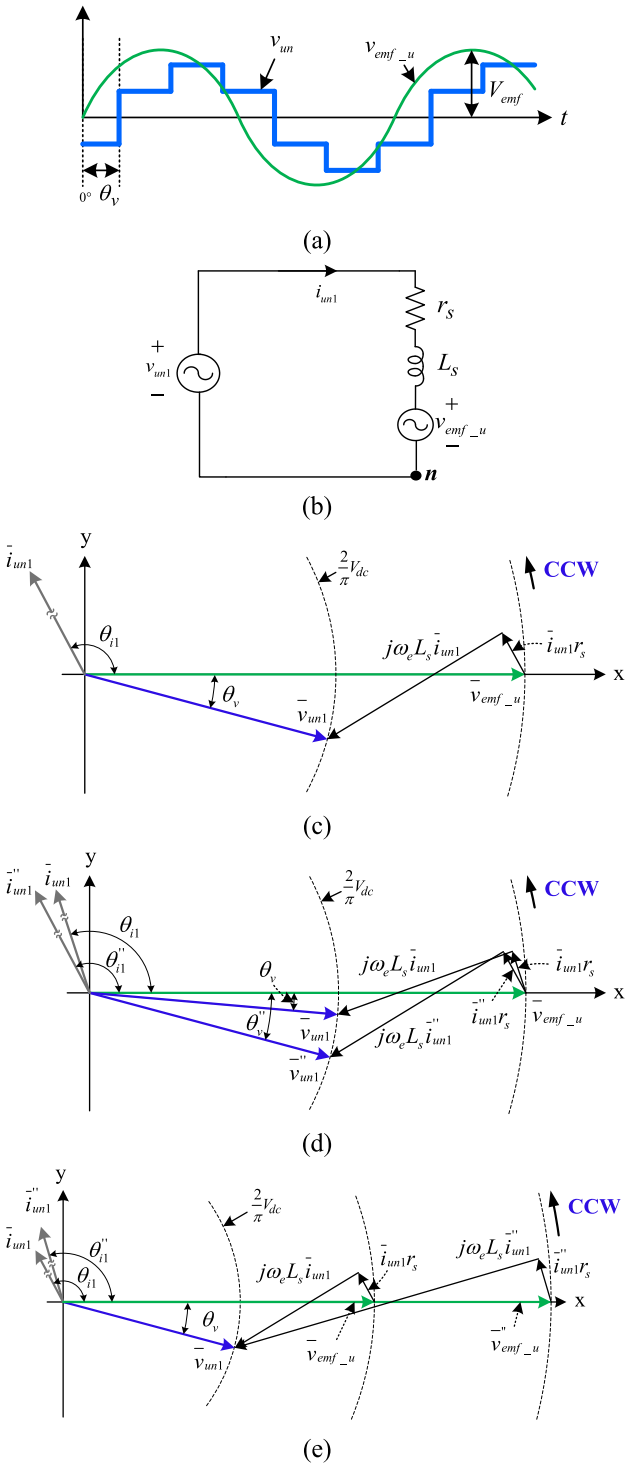

FIGURE 2. The u-phase equivalent circuit; (a) waveforms of no load back-EMF and phase voltage, (b) equivalent circuit of fundamental frequency, (c) phasor diagram of fundamental frequency, (d) phasor diagram at different θ_v under the same speed, (e) phasor diagram at the same θ_v under different speed.

Hence, the three phase generated average power P can be expressed as:

$$P \approx \frac{3}{\pi} V_{dc} k_e \frac{\phi_m}{L_s} \cos(\theta_v - 90°) = \frac{3}{\pi} V_{dc} k_e \frac{\phi_m}{L_s} \sin(\theta_v) \qquad (7)$$

The following phenomena can be observed from (4) to (7) and Fig. 2 when the ISG is operated in generating mode. (i) P is proportional to I_{un1} and $\cos(\theta_v - \theta_{i1})$ under fixed dc-link voltage, wherein I_{un1} and θ_{i1} can be derived as a function of ω_e (or engine speed) and θ_v. (ii) P is only controlled by θ_v in the high speed region, which means that the constant generated average power P can be achieved by keeping θ_v constant no matter how speed changes in the high speed region. Moreover, I_{un1} and θ_{i1} are also kept constant and are independent of power at high speeds.

TABLE 2. Specifications of the ISG.

Parameter	Value
Rated power (W)	300
Maximum speed (rpm)	8000
Number of pole pairs	6
Stator inductance (μH)	298
Phase resistance ($m\Omega$)	80.5
Phase back-EMF voltage (V_{rms} /1000rpm)	5.06

Based on (1) and (4), the equivalent circuit shown in Fig. 2(b) and the parameters of the ISG listed in Table 2, the simulation results among P, θ_v, and engine speed ω_r are shown in Fig. 3. The results indicate that: (i) the relationship between P and θ_v is nearly linear at fixed speed (3000rpm); (ii) P and I_{un1} are nearly constant under fixed θ_v when the engine speed is higher than 4000 rpm. Therefore, the results are consistent with the derived equations (5) and (7).

Since loaded condition in dc-link of the scooter is between 25W and 130W, θ_v can be between $2°$ and $-15°$ over a wide speed range by the simulation results, which means one should control θ_v carefully for reducing calculation error of θ_v to yield the required power.

III. PROPOSED CONSTANT VOLTAGE CONTROL UNDER GENERATING MODE

The proposed ISG control scheme is shown in Fig. 4, in which, the controller provides both vector control and six-step voltage control for cranking the engine and generating electric power, respectively. The gating signals for MOSFETs are selected by SW, where $\overline{V^*_{six}}$ and $\overline{V^*_{pwm}}$ are six-step voltage and PWM commands, respectively. Since cranking method for the ISG is well-known technology [8]–[10], this paper mainly focuses on the six-step voltage operation under generating mode with or without the battery. In addition, SW1 shown in Fig. 4 is arranged to let the battery be disconnected or connected to the dc-link for further testing. Due to higher pole pairs of the tested ISG, electric angle θ_e can be generated by electric angle estimator which is based on the u phase Hall sensor signal H_u. Fig. 5 shows θ_e and H_u with respect to u-phase back-EMF v_{emf_u}, wherein, the electric angle θ_e can be expressed as:

$$\theta_e = \frac{t}{T_{k-1}} \times 360° \qquad (8)$$

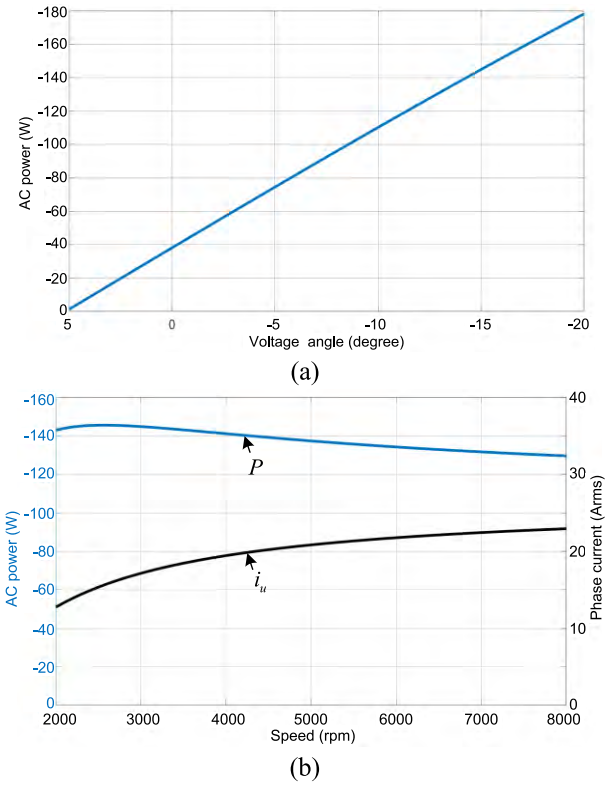

FIGURE 3. Simulation results of P and i_u at $V_{dc} = 12V$: (a) P vs. θ_V at 3000rpm; (b) P and i_u vs. speed at fixed $\theta_V (= -15°)$.

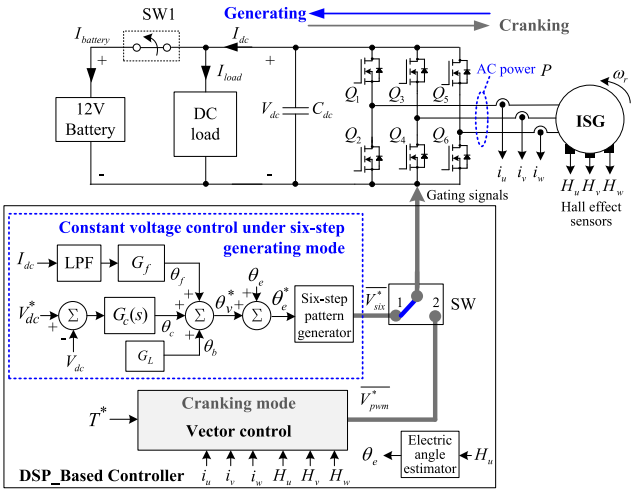

FIGURE 4. Proposed control methodology for ISG.

where T_{k-1} is the last back-EMF time period. Furthermore, Table 3 displays the output patterns of gating signals $\overline{V^*_{six}}$ for turning on or off MOSFETs Q_1, Q_3 and Q_5, which are generated by a six-step pattern generator according to θ^*_e. The gating signals for Q_1 and Q_2 are complementary, as are the gating signals for Q_3 and Q_4, and for Q_5 and Q_6.

The control schemes of the generating mode are described as follows:

TABLE 3. $\overline{V^*_{six}}$ outputs by six-step pattern generator.

	θ^*_e					
	0° ≀ 60°	60° ≀ 120°	120° ≀ 180°	180° ≀ 240°	240° ≀ 300°	300° ≀ 360°
Q_1	ON	ON	ON	OFF	OFF	OFF
Q_3	OFF	OFF	ON	ON	ON	OFF
Q_5	ON	OFF	OFF	OFF	ON	ON

(i) The voltage phase command θ^*_v is generated by a dc-link current feedforward module G_f, a dc-link voltage controller $G_c(s)$, and a light load feedforward angle control G_L. θ^*_v and electric angle command θ^*_e are arranged as:

$$\theta^*_v = \theta_b + \theta_c + \theta_f \tag{9}$$
$$\theta^*_e = \theta^*_v + \theta_e \tag{10}$$

where

θ_b is phase angle for light load; θ_c and θ_f are generated by $G_c(s)$ and G_f, respectively.

Hence, the generated power of the ISG is controlled by θ^*_v according to (4) to fulfil a constant dc-link voltage control over wide engine speeds.

(ii) Voltage controller $G_c(s)$ is adopted to both stabilize dc-link voltage and reduce the effects of electric parameters variations caused by flux saturation and/or operating temperature change.

(iii) The dc-link current feedforward module G_f is used to reach good load regulation of the dc-link voltage under a step load change without 12V battery, such as a headlight turn-on or turn-off, by detecting the dc-link current I_{dc}. The θ_f can be derived from (4) by neglecting the rectifier loss:

$$\theta_f = G_f(I_{dc}) \approx \cos^{-1}\left(\frac{\pi I_{dc}}{3I_{un1}}\right) + \theta_{i1} \tag{11}$$

Moreover, a low-pass filter (LPF) is used to rectify the current ripple induced by the six-step voltage operation. The cutoff-frequency of the LPF can be tuned on-line according to the ISG speed to enhance load regulation of V_{dc}. The simulation results of θ_f under different speeds and values of I_{dc} are shown in Fig. 6.

(iv) The feedforward angle θ_b yielded by G_L is utilized to provide small generated power (25W) for the fuel injection pump and ignition. From which, the voltage controller $G_c(s)$ can be easily adjusting to achieve better dc-link voltage control in steady state. Actually, θ_b and θ_f are obtained from (4), except that θ_b is set as 2° to provide stable minimal power, which can avoid reading small but noisy dc-link current.

In order to analyze stability of the proposed voltage controller, small-signal transfer functions are derived at the operating point according to Fig. 7 and (7), assuming that the electric parameters, such as k_e, ϕ_m, and L_s of the ISG,

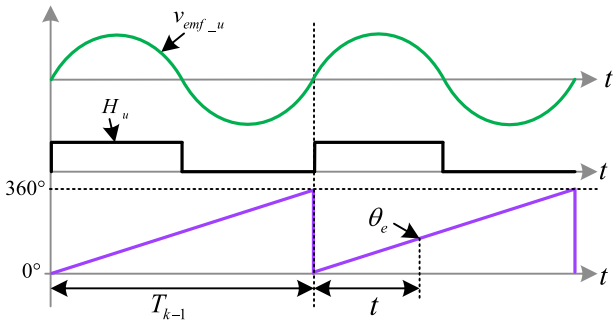

FIGURE 5. Hall sensor signal with respect to u-phase back-EMF.

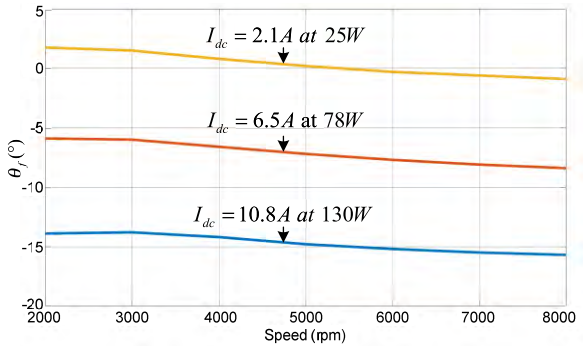

FIGURE 6. Simulation results of θ_f under different engine speeds and values of I_{dc}.

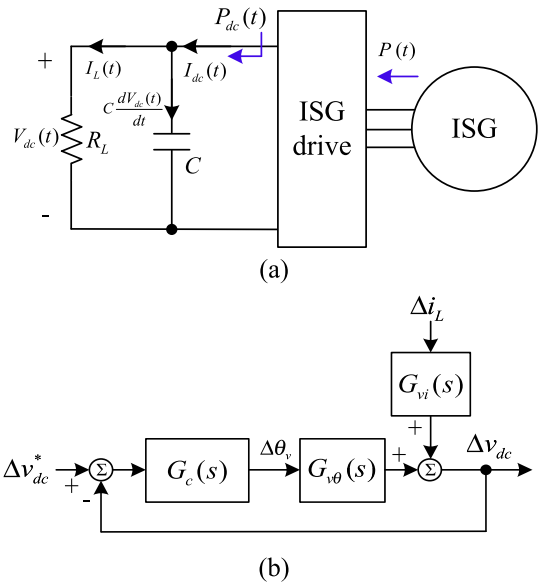

FIGURE 7. Small signal modeling; (a) equivalent circuit, (b) function block.

are unchanged. Hence, we have

$$P_{dc}(t) = \bar{P}_{dc} + \Delta p_{dc}(t) = V_{dc}(t)[I_L(t) + C\frac{dV_{dc}(t)}{dt}] \quad (12)$$

$$P(t) = \bar{P} + \Delta p(t) = \frac{3}{\pi}V_{dc}(t)k_e\frac{\phi_m}{L_s}\sin[\theta_v(t)] \quad (13)$$

where

$X(t)[= \bar{X} + \Delta x(t)]$: time-varying signal

$\bar{X}$: operating point

$\Delta x(t)$: small signal or ac term

If we neglected the second-order ac terms and $\bar{\theta}_v$ is small in the operating speed range, then

$$\Delta p_{dc}(t) = (I_L + sCV_{dc})\Delta v_{dc} + V_{dc}\Delta i_L \quad (14)$$

$$\Delta p(t) \approx (K\sin\bar{\theta}_v)\Delta v_{dc} + (K\bar{V}_{dc}\cos\bar{\theta}_v)\Delta\theta_v$$
$$\approx (K\sin\bar{\theta}_v)\Delta v_{dc} + KV_{dc}\Delta\theta_v \quad (15)$$

where

$$K = \frac{3}{\pi}\frac{\lambda_m}{L_s}$$

With the approximation $\Delta p_{dc}(t) \approx \Delta p(t)$, one obtains

$$\Delta v_{dc}(s) = G_{v\theta}(s)\Delta\theta_v(s) + G_{vi}(s)\Delta i_L(s) \quad (16)$$

The closed-loop transfer function is

$$\Delta v_{dc}(s) = \frac{G_c(s)G_{v\theta}(s)}{1+G_c(s)G_{v\theta}(s)}\Delta v_{dc}^*(s) + \frac{G_{vi}(s)}{1+G_c(s)G_{v\theta}(s)}\Delta i_L(s) \quad (17)$$

where

$$G_{v\theta}(s) = \frac{K}{sC + (\frac{\bar{I}_L}{\bar{V}_{dc}} - \frac{K}{\bar{V}_{dc}}\sin\bar{\theta}_v)}$$

$$G_{vi}(s) = \frac{-1}{sC + (\frac{\bar{I}_L}{\bar{V}_{dc}} - \frac{K}{\bar{V}_{dc}}\sin\bar{\theta}_v)}$$

$$G_c(s) = K_p + \frac{K_i}{s}$$

Hence, the characteristic function of (17) can be derived

$$C\overline{V}_{dc}s^2 + (\bar{I}_L + KK_p\overline{V}_{dc} - K\sin\bar{\theta}_v)s + KK_i\overline{V}_{dc} = 0 \quad (18)$$

From (18), one can make the following inferences: (i) $\bar{\theta}_v$ is negative in generating mode, which means the proposed voltage controller will make the system stable; (ii) although $\bar{\theta}_v$ may be positive for the practical system shown in Fig. 6 under a low engine speed and light load, the system will be stable by tuning the gains of $G_c(s)$.

IV. EXPERIMENTAL RESULTS

In order to verify effectiveness of the proposed method, test results are made by ISG drive on the test bench and a 150cc scooter. The DSP-based ISG drive was built and all the control algorithms are implemented by the DSP. Fig. 8 shows the experimental setup of the ISG test bench and scooter. A PMSM motor drive system serves as the active load, which provides speed control to simulate engine operation for validating the proposed system on the test bench. The generated ac power of ISG is measured by a power meter (WT 1600, Yokogawa).

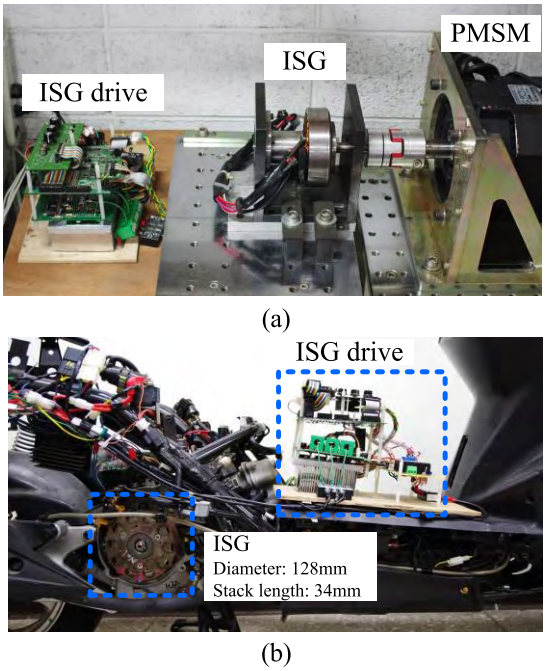

FIGURE 8. Experimental setup; (a) the ISG test bench, (b) the ISG system is installed and tested in a 150cc scooter.

A. VERIFICATION BY TEST BENCH

1) GENERATED POWER VS. SPEED AND θ_V

Fig. 9 shows tested results of phase voltage v_u, phase current i_u, θ_v, and no load back-EMF angle θ_{emf} generated by software according to Hall effect sensors at 3000rpm and 102W ac generated power. Although the drive output voltage is operated in six-step mode, the total harmonic distortion (THD) of i_u is less than 4.1%.

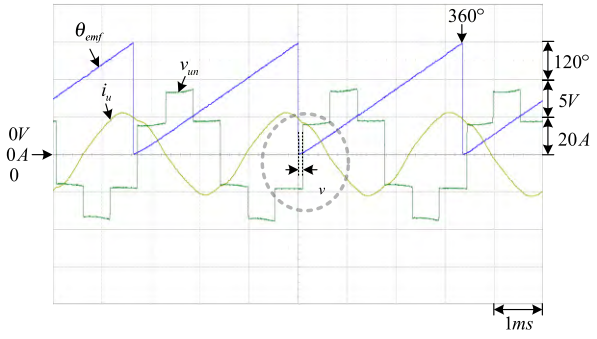

FIGURE 9. Measured results of v_u, i_u, θ_v, and no load back-EMF angle θ_{emf} at 3000rpm and 102W.

The simulation and measured results of P, engine speed and θ_v are shown in Fig. 10, wherein, the measured results are close to simulation results. The inductances of the ISG are measured by reactive power using a 20Arms/200Hz current source. Hence, the measured average inductance ($298\mu H$) is set for simulation which had accounted for the flux saturation effect by a larger current to reduce the error between simulation and measurement.

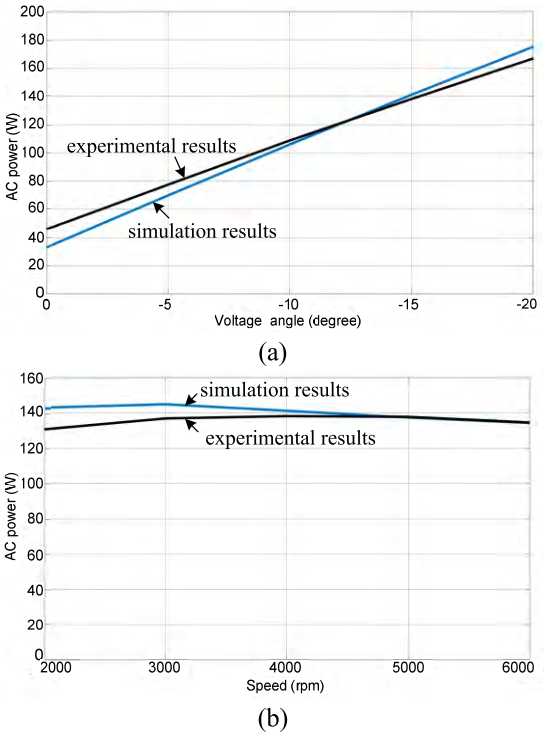

FIGURE 10. Simulation and measured results of P, speed and θ_V; (a) P at 4000rpm with different values of θ_V, (b) P at $\theta_V = -15°$ with different operating speeds.

2) VOLTAGE CONTROL

Let the ISG be stably operated at 4000 rpm and 130W dc load by the proposed six-step voltage operation with voltage compensator $G_c(s)$ only; hereafter, the battery is disconnected. Fig. 11 shows the measured results which V_{dc} can be controlled at 12V and the peak-to-peak voltage ripple is less than 1.5V without the battery. Fig.12 shows the measured results of the step load change from 25W to 130W; the dip and overshoot of the dc-link voltage are less than 1V and there is a nearly 2A charging current for the battery simultaneously. One should be aware that the battery provides a favorable energy buffer to reduce the dc-link voltage ripple and the effect of the step load change.

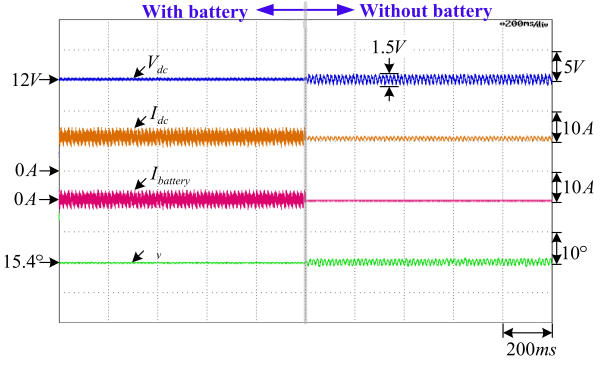

FIGURE 11. Measured results of voltage control with and without the battery at 4000rpm/130W dc load.

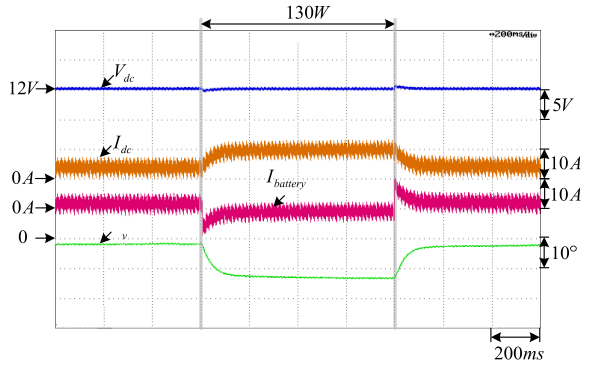

FIGURE 12. The experimental results of step load change (25W to 130W and vice versa) with battery @ 4000rpm.

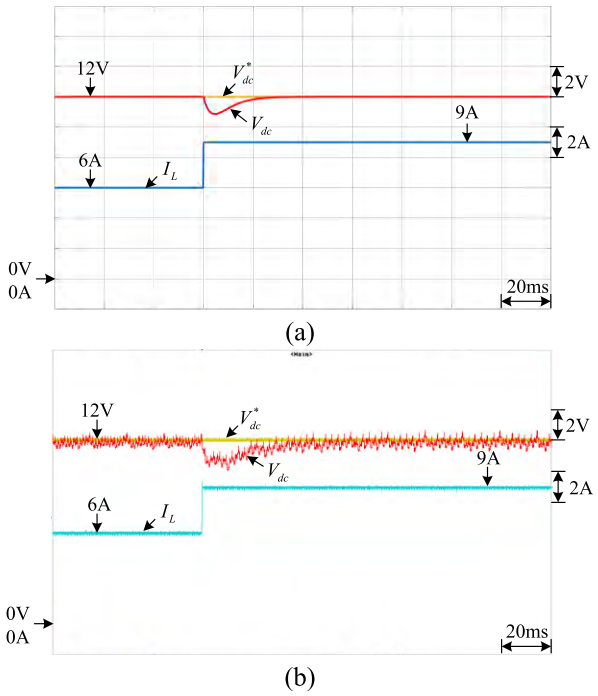

FIGURE 13. Step-load regulation ($V_{dc}^* = 12V$, $\bar{\theta}_v = -5°$, 4000rpm); (a) simulation result, (b) experimental result.

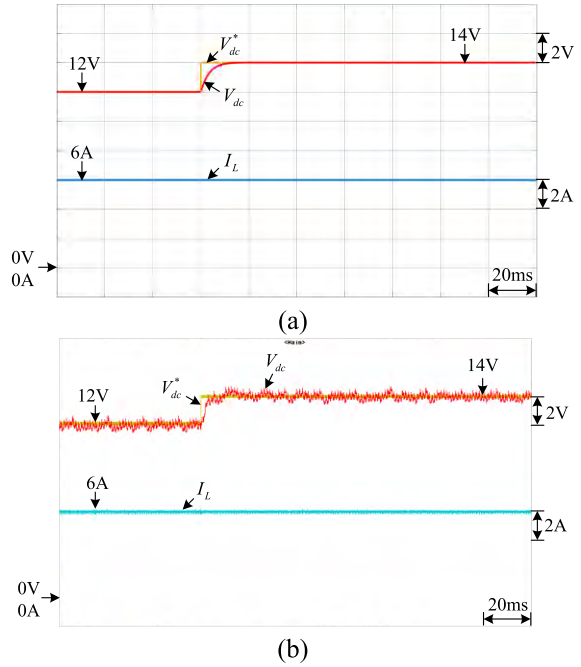

FIGURE 14. Voltage command tracking ($V_{dc}^* = 12V$ to 14V, $\bar{\theta}_v = -5°$, 4000rpm); (a) simulation result, (b) experimental result.

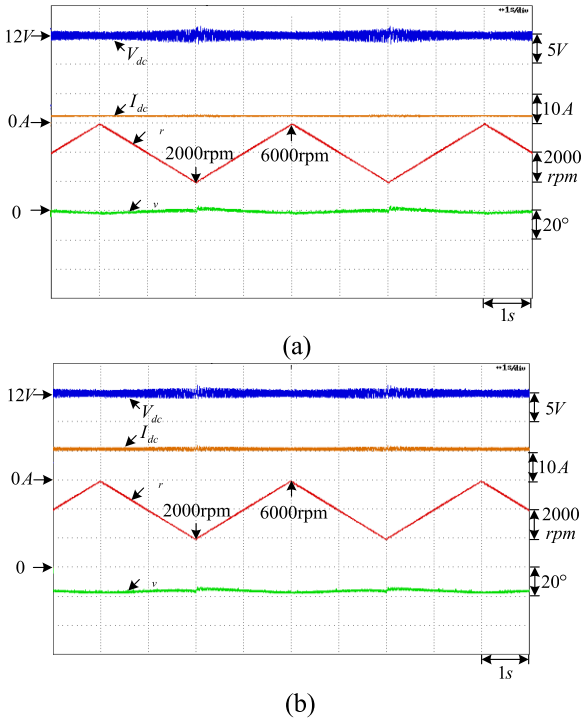

FIGURE 15. Constant dc voltage control under speed variation by proposed control methodology without the battery under different load conditions:F (a)25W, (b)130W.

Fig. 13 and 14 show simulation results and experimental results of load regulation and voltage command tracking. One should be aware that the experimental results are close to simulation results; wherein, $G_c(s) = 0.035 + \frac{5.76}{s}$ leads the crossover frequency to be 1000Hz and phase margin to be 90°. Moreover, under the same K_i and $\bar{\theta}_v = 5°$, the proposed system is still stable when $K_p \geq 0.0073$.

3) FEEDFORWARD CONTROL WITHOUT BATTERY

The derived control scheme also allows the dc-link voltage to be maintained a 12V under triangle-type speed variations from 2000 rpm to 6000 rpm at 25W and 130W without the battery, as shown in Fig. 15. The step load change from 25W to 130W and vice versa are added on the ISG operated at 4000rpm without the battery, the measured waveforms are shown in Fig.16. Fig.16(b) shows that adding the proposed feedforward angle θ_f will effectively reduce the dc-link voltage variation from 4V to nearly 0V during step load change.

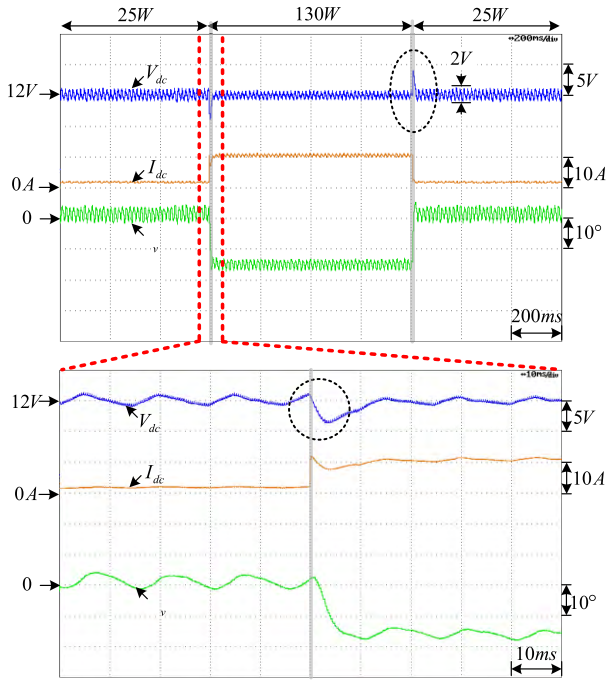

(a)

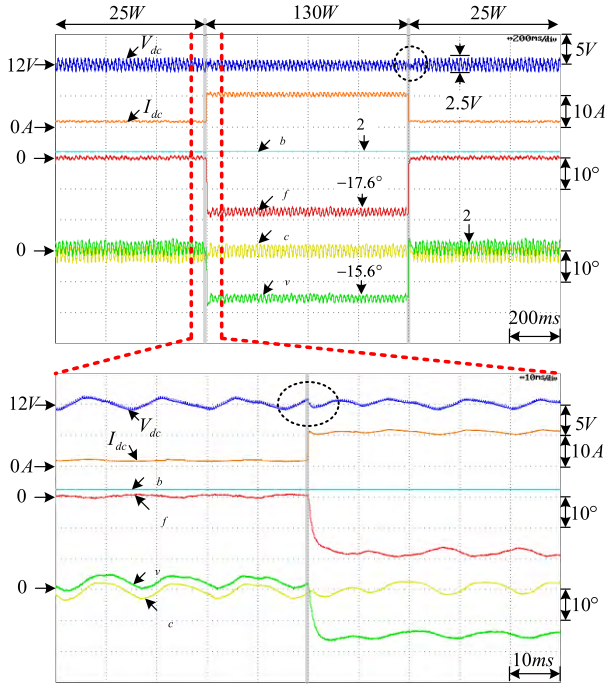

(b)

FIGURE 16. The experimental results of step load change (25W to 130W) without battery @4000rpm; (a) without feedforward and zoom in, (b) with feedforward and zoom in.

B. TESTING THE ISG ON A 150CC SCOOTER

Due to pulsating speed caused by the ICE, we need to test the ISG on a 150cc scooter to verify the proposed control scheme. The step load change is the same as the ISG test bench for comparison.

1) CRANKING TEST

Fig. 17 shows the test results of a 150cc scooter with the battery from cranking the engine to generating mode. It spends 850ms to allow the engine precede from stop to generating mode; vector control also works well for cranking the engine. For a well-tuned mass-produced scooter, the cranking time could be less than 0.5s compared with the tested prototype scooter.

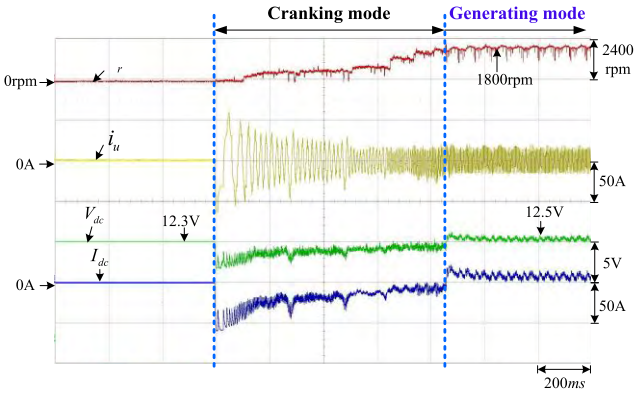

FIGURE 17. Measured results of a 150cc scooter from cranking engine to generating mode.

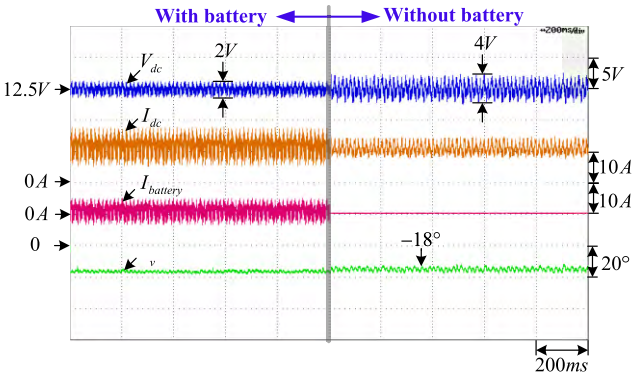

FIGURE 18. Measured results of voltage control with and without the battery at 4000rpm/130W dc load.

2) VOLTAGE CONTROL WITH OR WITHOUT BATTERY

Let the engine be stably operated at approximately 4000rpm by throttle and 130W dc load supplied by the proposed six-step voltage operation with voltage compensator $G_c(s)$ only; hereafter, the battery is disconnected. Fig. 18 shows the measured results where V_{dc} can be controlled at 12V and the peak-to-peak voltage ripple is less than 4V without the battery. The larger voltage and current ripple compared with Fig.11 might be caused by the pulsating speed of the ICE. Moreover, the proposed system also provides good dc-link voltage control during engine acceleration from 2000rpm to 6200rpm without the battery as shown in Fig. 19.

3) FEEDFORWARD CONTROL WITHOUT BATTERY

Without the battery, the measured results of step load change from 25W to 130W and vice versa at 4000rpm are shown

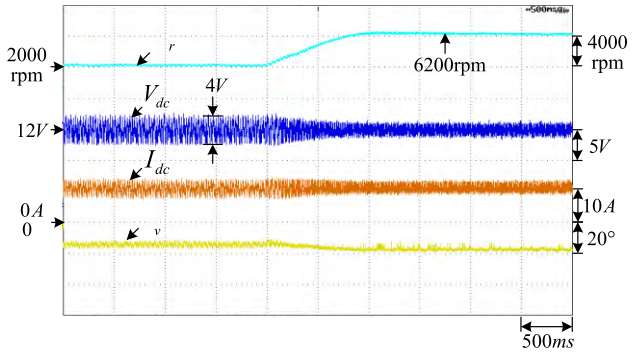

FIGURE 19. Constant dc voltage control by the proposed control scheme at 130W dc load without the battery during engine acceleration from 2000 rpm to 6200 rpm.

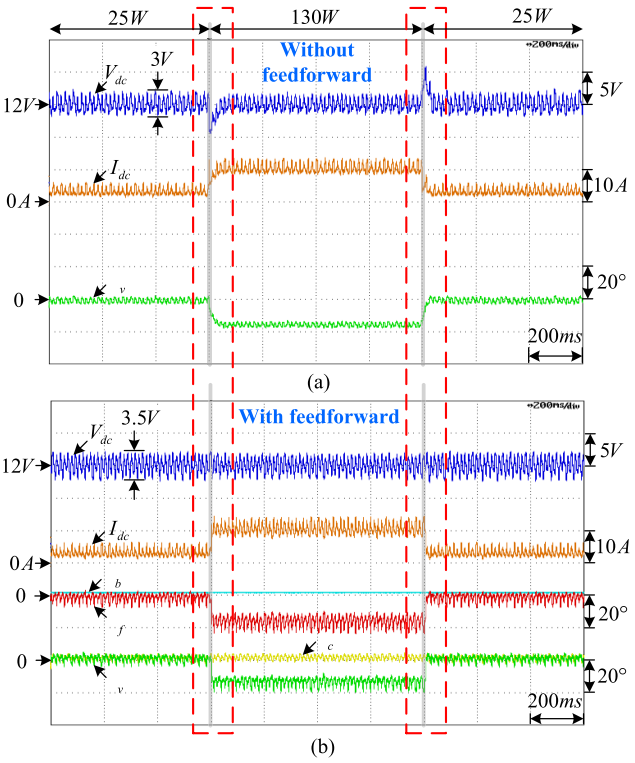

FIGURE 20. Experimental results of step load change from 25W to 130W and vice versa on a 150cc scooter without the battery; (a) without feedforward, (b) with feedforward at 4000rpm.

in Fig. 20. Fig. 20(b) shows results similar to Fig. 16(b), such that adding the proposed feedforward angle θ_f will reduce the dc voltage variation at step load change without the battery.

V. CONCLUSION

A dc-link voltage control method for a PMSM type ISG for generating 12V dc voltage over a wide range of engine speeds for an idling-stop scooter was proposed. The six-step voltage operation in generating mode was applied and a phasor diagram based on fundamental frequency was used to explain that the phase voltage lagging behind the same phase back-EMF by θ_v can achieve the required power generation under wide engine speeds, even without the 12V battery. Experimental results were carried out to show the following advantages of the proposed method in generating mode on both the ISG test bench and a 150cc scooter:

(i) The dc-link voltage can be kept at 12V under 2000rpm to 6000rpm engine speed with or without the 12V battery on the ISG test bench and a 150cc scooter at 130W. Moreover, dc- link voltage ripple (peak to peak) is less than 4V without the 12V battery.

(ii) The dc-link voltage variation under step load change from 25W to 130W and vice versa without the battery can be reduced to nearly zero by a dc-link current feedforward module.

(iii) The simulation results of the derived formulas are close to the experimental results in generated ac power under a wide range of engine speeds.

REFERENCES

[1] G. Friedrich and A. Girardin, "Integrated starter generator," *IEEE Ind. Appl. Mag.*, vol. 15, no. 4, pp. 26–34, Jul. 2009.

[2] Natural Resources Canada. (2018). *Learn the Facts: Idle Stop-Start Technology and Its Effect on Fuel Consumption*. [Online]. Available: http://www.nrcan.gc.ca/energy/efficiency/transportation/cars-light-trucks/buying/16757

[3] HONDA. (2018). *What is the Idling Stop System*. [Online]. Available: http://world.honda.com/motorcycle-picturebook/idling-stop/index.html

[4] C.-H. Yu, C.-T. Tseng, and S.-C. Chuang, "Evaluation of fuel economy and emissions reduction for a motorcycle with automatic idling-stop device," *ASME. J. Energy Resour. Technol.*, vol. 136, no. 2, p. 021206, 2014.

[5] I. A. Viorel, L. Szabó, L. Löwenstein, and C. Şteţ, "Integrated starter-generators for automotive applications," *Acta Electrotehnica*, vol. 44, no. 3, pp. 255–260, 2004.

[6] G.-H. Lee, G.-S. Choi, and W. Choi, "Design considerations for low voltage claw pole type integrated starter generator (ISG) system," *J. Power Electron.*, vol. 11, no. 4, pp. 527–532, 2011.

[7] S. Saponara, P. Tisserand, P. Chassard, and D.-M. Ton, "Design and measurement of integrated converters for belt-driven starter-generator in 48 V micro/mild hybrid vehicles," *IEEE Trans. Ind. Appl.*, vol. 53, no. 4, pp. 3936–3949, Jul./Aug. 2017.

[8] J. Zhang and M. F. Rahman, "A direct-flux-vector-controlled induction generator with space-vector modulation for integrated starter alternator," *IEEE Trans. Ind. Electron.*, vol. 54, no. 5, pp. 2512–2520, Oct. 2007.

[9] A. K. Jain, S. Mathapati, V. T. Ranganathan, and V. Narayanan, "Integrated starter generator for 42-V powernet using induction machine and direct torque control technique," *IEEE Trans. Power Electron.*, vol. 21, no. 3, pp. 701–710, May 2006.

[10] J. Wai and T. M. Jahns, "A new control technique for achieving wide constant power speed operation with an interior PM alternator machine," in *Proc. Conf. Rec. IEEE IAS Annu. Meeting*, vol. 2, Sep./Oct. 2001, pp. 807–814.

[11] C. Liu, K. T. Chau, and J. Z. Jiang, "A permanent-magnet hybrid brushless integrated starter–generator for hybrid electric vehicles," *IEEE Trans. Ind. Electron.*, vol. 57, no. 12, pp. 4055–4064, Dec. 2010.

[12] G. Friedrich, L. Chedot, J. M. Biedinger, and P. Macret, "Integrated starter generator: Need of an optimal design and control approach. Application to a permanent magnet machine," in *Proc. IEEE Int. Conf. Elect. Mach. Drives*, May 2005, pp. 1529–1534.

[13] M. Barcaro, A. Faggion, L. Sgarbossa, N. Bianchi, and S. Bolognani, "Performance evaluation of an integrated starter alternator using an interior permanent magnet machine," *IET Electr. Power Appl.*, vol. 4, no. 7, pp. 539–546, Aug. 2010.

[14] J.-H. Seo, S.-M. Kim, and H.-K. Jung, "Rotor-design strategy of IPMSM for 42 V integrated starter generator," *IEEE Trans. Magn.*, vol. 46, no. 6, pp. 2458–2461, Jun. 2010.

[15] C. Feng, P. Yulong, L. Xinmei, G. Bin, and C. Shukang, "The performance research of starter-generator based on reluctance torque used in HEV," *IEEE Trans. Magn.*, vol. 45, no. 1, pp. 635–638, Jan. 2009.

[16] J. Wei, Q. Deng, B. Zhou, M. Shi, and Y. Liu, "The control strategy of open-winding permanent magnet starter-generator with inverter-rectifier topology," *IEEE Trans. Ind. Informat.*, vol. 9, no. 2, pp. 983–991, May 2013.
[17] K. T. Chau, Y. B. Li, J. Z. Jiang, and C. Liu, "Design and analysis of a stator-doubly-fed doubly-salient permanent-magnet machine for automotive engines," *IEEE Trans. Magn.*, vol. 42, no. 10, pp. 3470–3472, Oct. 2006.
[18] P. Bajec, B. Pevec, D. Voncina, D. Miljavec, and J. Nastran, "Extending the low-speed operation range of PM Generator in automotive applications using novel AC-DC converter control," *IEEE Trans. Ind. Electron.*, vol. 52, no. 2, pp. 436–443, Apr. 2005.
[19] I. Petrov and J. Pyrhonen, "Performance of low-cost permanent magnet material in PM synchronous machines," *IEEE Trans. Ind. Electron.*, vol. 60, no. 6, pp. 2131–2138, Jun. 2013.
[20] I. Petrov, M. Niemelä, P. Ponomarev, and J. Pyrhönen, "Rotor surface ferrite permanent magnets in electrical machines: Advantages and limitations," *IEEE Trans. Ind. Electron.*, vol. 64, no. 7, pp. 5314–5322, Jul. 2017.
[21] T. Yanagisawa, T. Yamanishi, K. Utsugi, and T. Nagatsuyu, "Development of idling stop system for 125 cm^3 scooters with fuel injection," SAE Paper 2010-32-0121.
[22] P. Chen, S. Chang, and R. Chen, "Decoupled self-tuning PI controller for an idling stop system applied to scooters," *Int. J. Automot. Technol.*, vol. 18, no. 4, pp. 663–670, 2017.

MING-SHI HUANG received the B.S. degree in electrical engineering from the National Taiwan University of Science and Technology, Taiwan, in 1987, the M.S. degree in electrical engineering from Tatung University, Taiwan, in 1991, and the Ph.D. degree in electrical engineering from National Tsing Hua University, Taiwan, in 2004.

From 1987 to 2004, he was a Researcher with the Mechanical Industry Research Laboratories, Industrial Technology Research Institute. He is currently an Associate Professor with the Department of Electrical Engineering, National Taipei University of Technology, Taipei, Taiwan. His areas of research interests include power electronics, variable-speed drives, and electrical power train in vehicle applications.

KUAN-CHENG CHEN received the B.S. and M.S. degrees in electrical engineering from the National Taipei University of Technology, Taiwan, in 2010 and 2013, respectively, where he is currently pursuing the Ph.D. degree. His research interests include motor control, power electronics, and digital control.

TSE-KAI CHEN received the B.S. degree in electrical engineering from Fu Jen Catholic University, and the M.S. degree in electrical engineering from the National Taipei University of Technology, Taipei, Taiwan, in 2015 and 2018, respectively. His research interests include power electronics and motor drives.

YU-CHIANG LIANG received the B.S. degree in mechanical engineering from National Central University, in 1981, and the M.S. degree in mechanical engineering from National Taiwan University, in 1986.

Since 1986, he has been with Sanyang Motor Co., Ltd., Hsinchu, Taiwan, where he is currently the Chief Researcher, and is responsible for the technology strategy and new technology development.

GUAN-YOU PAN received the B.S. degree in electrical engineering from the National Kaohsiung University of Science and Technology, Taiwan, in 2009, and the M.S. degree in applied electronics technology from National Taiwan Normal University, in 2011.

Since 2011, he has been with the Sanyang Motor Co., Ltd., Hsinchu, Taiwan, where he is currently with the Mechatronic Control Department. His research interests include controller design for electric scooter and ISG drives for scooter.